<u>3D MICROSTRUCTURE MODELING OF LONG FIBER REINFORCED THERMOPLASTICS</u>

S. Fliegener[a], M. Luke[a], P. Gumbsch[a,b]

Corresponding author: S. Fliegener, sascha.fliegener@iwm.fraunhofer.de

a) Fraunhofer Institute for Mechanics of Materials IWM, Freiburg, Germany

b) Institute for Applied Materials, Karlsruhe Institute of Technology KIT, Germany

Abstract: A novel procedure for the generation of a representative volume element for long fiber reinforced thermoplastics and materials with a similar microstructure is presented here. It is characterized by a maximum fiber aspect ratio of approx. 5000 and a maximum fiber volume fraction up to 25 %. The modeling procedure is based on characteristic values describing the microstructure in a statistical sense, which are the fiber orientation distribution, the fiber length distribution and the fiber volume content. The resulting mesh for finite element analysis represents the microstructure with a relatively low element count, modeling each fiber only by a single element per cross section. Hence, the model is computationally very efficient and allows the analysis of comparably large structures which include the complete fiber length spectrum of the investigated material. The procedure is validated against the elastic properties of three material variants with different fiber volume fractions, incorporating their experimental measured fiber orientation and length distributions.

Keywords: A. Polymer-matrix composites (PMCs), B. Elastic Properties, B. Finite element analysis (FEA), B. Multiscale modeling

1. Introduction

High-performance cost-efficient composite materials which can be manufactured on mass-production scale are needed e.g. for lightweight automotive components. Long-fiber reinforced thermoplastics (LFT) are extremely promising in this respect since they are well suited for mass production by injection or compression molding. Automotive applications, however, require that these materials and their mechanical performance must be simulated which in turn requires precise microstructure based modeling of their effective behavior. Such modeling is also needed to optimize material design or processing conditions.

A variety of analytical approaches is available [1] to predict the effective elastic properties of short fiber composites. Most approaches are based on Eshelby's equivalent inclusion problem [2], which treats an ellipsoidal inclusion in an infinite matrix at dilute concentration. The Mori-Tanaka model [3] extends the Eshelby problem to non-dilute concentrations of the inclusions by considering phase interactions in an approximate way. The elastic constants of a unidirectional composite can be determined in this way [4]. Following a different route one can start from Hill's self-consistent scheme [5] and derive the modeling of transversely isotropic composites including the effects of fiber aspect ratio, which leads to the Halpin-Tsai equations [6]. The effect of fiber orientation distribution can be included by averaging the elastic constants of a transversely isotropic composite [7]. All these analytical models suffer from the drawback that they require significant simplifications regarding the geometry and the interactions between fibers or inclusions. Nevertheless, the orientation averaging scheme yields accurate results for the elastic properties of LFTs [8,9]. However, geometrical features like fiber waviness resulting from the dense packing of the LFT microstructure and detailed fiber-fiber interactions in regions of high fiber density cannot be addressed by the classical analytical approaches. In order to overcome these restrictions, a micromechanical model is needed which explicitly depicts the complex microstructure of such materials. This is particularly important when modeling the complex nonlinear and time-dependent behavior of the thermoplastic matrix of LFTs as well as fiber-matrix interface debonding phenomenae. Finite element (FE) models are generally capable to fulfill such tasks. Gusev *et al.* demonstrated this for straight short fiber composites under variation of the fiber orientation distribution and found agreement of the elastic properties with the analytical solutions within engineering accuracy [10]. They also studied the effects of fiber volume fraction, aspect ratio and fiber length distribution on the elastic and thermoelastic properties of short fiber composites [11]. In a similar spirit, Pan *et al*. created a representative volume element (RVE) for random chopped fiber composites with volume fractions up to 35 % and applied the model to predict the elastic properties as well as the damage behavior [12, 13]. Harper *et al*. modeled discontinuous carbon fiber composites with unlimited volume fraction by representation of the fibers as one dimensional beam elements, embedded in a free or structured matrix mesh [14]. Harper systematically investigated the effects of RVE size, boundary conditions, fiber length (up to 10 mm) and volume fraction (up to 50 %) on the elastic properties of structures with random orientation. The main advantage of the latter method is the ease of implementation as well as its computational efficiency, while limitations exist with respect to application to the modeling of material and in particular interface failure. Soltani *et al*. reconstructed a 3D representation of non-woven fabrics with algorithms applied on 2D slices of CT voxel data to calculate the permeability of such fiber networks [15]. Each fiber features the exact geometry as observed by the CT scan. However, vast efforts have to be made for such reconstruction mainly due to detailed checks of neighborhood relations for each voxel. For the extremely high aspect ratio of LFT, such detailed reconstruction of CT data can be considered as problematic due to the data amount and the necessity to acquire CT scans with a huge volume with the lowest limit being the maximum fiber length. With state-of-the-art CT and computational resources, this cannot be considered as currently technically feasible. Faessel *et al*. generated fiber networks based on measured statistical values describing the microstructure (fiber orientation, density, length and curvature) and investigated the effects on thermal conductivity [16]. However, the procedure does not account for any matrix material and permits fiber interpenetration.

In summary, no suitable microstructure generation method for LFTs with respect to representation of high aspect ratio fibers, the matrix as well as the fiber-matrix interface is currently presented in literature. Modeling LFTs is particularly challenging since their mechanical properties strongly depend on all their microstructural characteristics (fiber length distribution, fiber orientation distribution, fiber volume ratio). In detail, the fiber length distribution of LFTs can reach values of maximum fiber aspect ratio in the region of 5000 while typically also a large fraction of short fibers is present. As a consequence, the resulting RVE for the FE model must be large enough to include the complete spectrum of fiber lengths. The microstructure must therefore be modeled in a very efficient way to limit the element count to a reasonable value. The key approach of the work presented here is to build up a fully three dimensional LFT microstructure by modeling the fibers with only a single hexahedral element over their cross section and accounting for the matrix by a mesh of tetrahedral elements in which the element size can grow dynamically in regions of locally decreasing fiber density. To demonstrate the applicability of this model it is used to predict the elastic properties of three different LFT materials based on experimentally determined microstructural properties and the properties of the constituent phases. The model can of course be extended to include the non-linear behavior of the thermoplastic matrix and the effects of material and/or interface damage. It can then be used for the development and validation of effective models at the homogenized / smeared level which are suited for structural simulation of LFT parts and components.

2. Investigated material

The investigated LFT material consists of a polypropylene matrix (*DOW® C711-70RNA*) and glass fibers (*TufRov® 4575*). Three material variants with different fiber fractions (PPGF30, PPGF20 and PPGF10) have been produced. PPGF30 (30 wt-%, 13.2 vol-%) and PPGF20 (20 wt-%, 8.2 vol-%) are of great interest for structural application and commonly used by the automotive industry, while PPGF10 (10 wt-%, 3.8 vol-%) is rather of academic interest and provides additional data for model validation. In order to produce the LFT strand as the pre-product of the process, the fiber rovings were fed into a double screw extruder and mixed with the polypropylene melt. The overlapping edges of the co-rotating screws break the fibers into fragments with a maximum length defined by the pitch of the screws. The material resulting from this so called direct LFT process [17,18] is characterized by a broad fiber length distribution reaching from a large amount of fiber fragments well below 1 mm to very long fibers up to 50 mm in length. Plates with dimensions of 400 x 400 x 3 mm^3 were produced by compression molding in the following step. The LFT strand as it came out of the extruder was placed asymmetrically into the mold. The material flow during the compression of the mold generates a high degree of fiber orientation outside the strand inlay position. This so-called flow region of the plate is investigated in the following and can be considered as the most relevant state of the material for applications.

3. Model generation

The modeling procedure is divided into three steps: First, a fiber generator tool creates a stack of planar fibers with given length and orientation distributions. This stack is then compressed until the desired fiber volume fraction is reached. In the last step, the remaining gaps are filled with elements representing the matrix to complete the RVE.

3.1. Generation of a fiber stack

The structure of the fiber generator tool is shown in Fig. 1 as a flowchart. The program generates a stack of layers in which each layer contains multiple planar, straight fibers according to the statistics provided by the user. These are the desired fiber orientation distribution $L(\alpha)_{des.}$, the desired fiber length distribution $L(l)_{des.}$, the desired total fiber length L_{tot}, the RVE dimensions X, Y, the limit of fiber length per layer L' as well as several other variables which control the process of the algorithm. The main aspects of the procedure are described in the following but details (e.g. to avoid endless loops) are omitted for reasons of clarity and comprehensibility.

First the length distribution $L(l)_{des.}$ describing the desired cumulative fiber length L for each length class l is scanned for the maximum value of l in which the desired value of L is still larger than the length sum of the currently generated fibers $\Sigma L(l)$. If necessary, the value of l is decreased until a length class is found which is not fully occupied. In the next step, a random in-plane fiber angle α_f is chosen and the orientation distribution $L(\alpha)_{des.}$ is checked whether the desired cumulative length L for each class of angle α is still larger than the current value of fiber length $\Sigma L(\alpha)$ plus the current fiber length l_f. If a value of α_f is found, but the fiber does not fit inside the RVE dimensions X and Y, re-orientation is attempted by choosing an alternative value of α_f. The practical meaning of this procedure is to prevent cropping of longer fibers and to preserve long fibers by aligning them preferably in the direction of the largest RVE dimension. This aspect is further analyzed in Section 5.1.

In the next step, a random value for the fiber layer coordinate z is chosen. If the cumulative length per layer $\Sigma L(z)$ plus l_f is larger than the length per layer limit L', another layer is randomly chosen. L' is given by the user as a parameter to control the packing density for each layer. The number of layers is calculated by dividing the total fiber length L_{tot} by L'. The planar fiber position, defined by the fiber start and end points x_s, y_s is chosen randomly within the RVE borders and the end points x_e, y_e are calculated. The fiber location is then checked for intersection with any other fiber of the current layer. If all checks are successfully passed, the fiber is generated. If L' is set to a high value, too many fibers are packed into too few layers and too many attempts are then needed to find a fiber position where no collision with any other fiber in the specific layer occurs. Consequently the calculation time for the fiber generation procedure raises drastically. If the value for *L'* is set too low, e.g. resulting in only a single fiber per layer, the fiber stack increases in height which increases the calculation time for the following fiber compression procedure. Fiber placement is repeated until the total generated fiber length reaches the desired amount L_{tot}. If the desired fiber length is generated, the program ends with the automatic generation of an *ABAQUS®* input file for the following step of fiber compression.

3.2. Fiber compression

The fiber stack is compressed by an explicit FE simulation until the desired value of the fiber volume fraction is reached. Fully integrated elements (C3D8) are used for fiber compression, while the element type is changed to reduced integration (C3D8R) for structural analysis. The procedure as well as the coordinate system which defines the mean fiber orientation as the flow direction (*1*), the perpendicular direction (*2*) and the layer stacking or pressing direction (*3*) is illustrated in Fig. 2. The fiber stack is placed in between two rigid shell elements whose distance is continuously decreased until the desired fiber volume fraction is reached. The typical values for the fiber volume fraction of LFT materials in applications for structural parts are in the range of 5 % to 25 %. Due to their non-unidirectional alignment, their high aspect ratio and fiber volume fraction the fibers cannot remain straight to realize the required dense packing. This has been investigated in detail by others [19,20] for randomly oriented fiber structures.

In order to retain the fiber orientation distribution as well as possible, the pressing procedure is divided into two phases with different boundary conditions (BC). In Phase A of the compression procedure, active for 90 % of the total displacement of the rigid plates u_{max}, all nodes of each fiber are constrained in their planar displacements u_1, u_2 whereas u_3 was left unconstrained. This ensures that the in-plane orientation distribution remains unchanged and fiber waviness develops only in thickness direction. For the structures presented here, the achievable fiber volume fraction at the end of phase A is 5 % to 7.5 % before the simulation aborts due to excessive element distortion. To generate a higher volume fraction, the fiber constraints must be relaxed. The following scenario for phase B allows reaching volume fractions up to 25 % (depending on the orientation distribution and aspect ratio) with only minor distortion to the planar orientation distribution. In phase B, only the nodes of the first and last element of each fiber are constrained by boundary conditions, which set their displacement in *2*-direction to zero and apply a non-zero velocity in *1*-direction. A certain value of velocity parallel to the mean fiber direction as well as a non-zero friction coefficient of the contact formulation is beneficial to keep fiber waviness low and avoid major distortion of the orientation distribution. The two phase procedure was found necessary to reach contact between the fibers before waviness is allowed to develop. To keep a minimum distance between all fibers the *general contact* formulation in *ABAQUS® Explicit* was given a non-zero value for the *global thickness* parameter and the *feature edge* parameter was enabled to avoid penetration of the fibers.

3.3. Meshing and boundary conditions

In the last step of the RVE generation procedure, the deformed fiber mesh is imported into the FE preprocessing software *HyperMesh* to fill the remaining gaps between the fibers with a tetrahedral mesh representing the matrix. First, the fiber mesh is placed into a cuboid with the desired dimensions of the RVE. The faces of the three dimensional fiber elements (C3D8R) act as seeds for the tetrahedral matrix elements (C3D4) in order to let the matrix mesh grow from each fiber surface. The desired element size of the matrix mesh is chosen automatically by the meshing algorithm resulting in small elements in regions near or between several fibers and larger elements towards the RVE borders, where the fiber density decreases. For the RVEs analyzed in this work, this resulted in less than 10 million elements. Details of the resulting mesh for RVEs of all three investigated fiber volume fractions are shown in Fig. 3 with a part of the matrix mesh removed. The corresponding fiber lattice (1/4 of the total RVE) is depicted in Fig. 4. Due to the complexity of the structure and the fact that the fibers need to be enclosed by the RVE boundary surfaces to create the matrix mesh, it was not possible to consider periodic BCs for the RVE simulations. Thus, displacement BCs are applied as illustrated in Fig. 5. To determine the stiffness, the displacement values for each node of the constrained region $u_1 \ldots u_n$ is set to zero for one side (A) and to an equal non-zero value for the opposite side (B) of the RVE. Two node sets outside the stress concentrations near the constrained borders have been defined. The resulting displacement values for each node of the node sets a and b have then been averaged: $\underline{u}_a = avg\ (u_{a,1} \ldots u_{a,n})$ resp. $\underline{u}_b = avg\ (u_{b,1} \ldots u_{b,n})$ with $avg()$ being the arithmetic mean and the engineering strain has been calculated by $\varepsilon = (\underline{u}_b - \underline{u}_a) / l_0$ with l_0 being the initial distance between the node sets a and b. The modulus has finally been calculated according to Hooke's law by calculation of the quotient of engineering stress and strain: $E = \sigma / \varepsilon$. The stress σ has been obtained by dividing the sum of nodal reaction force $F_B = \Sigma F_{B,1} \ldots F_{B,n}$ at the RVE border B by the initial RVE cross section area.

4. Results

4.1. Experimental determination of fiber orientation distribution

The fiber orientation distribution was extracted from characteristic specimens by means of image analysis of computer tomographic (CT) scans. A *Phoenix nanome|x 180NF* µCT device was used to acquire the scans with a voxel size of approx. 8 µm and a resolution of 360^3 voxels of the cubic analysis section of approx. 3^3 mm^3 to screen the specimens over their complete thickness. The specimens were taken from the same regions of the LFT plates as the tensile specimens. In the following step the CT data was analyzed with the plugin *Directionality* of the image processing software *ImageJ* / *Fiji* [21]. The raw CT voxel data was decomposed into 360 slices of 2D-images in which the planar fiber orientation distribution for each slice was analyzed (see Fig. 6). The overall orientation distribution was derived by averaging over all 360 histograms. This procedure can be applied because no significant change of fiber orientation over the specimen thickness could be observed (see Fig. 7). The distributions are interpreted as fiber length fraction per angle class as the software recognizes the amount of picture area with a preferred direction and does not perform any segmentation of fibers. Similar measurements with *ImageJ* have been presented by Graupner *et al.* [22]. Validation against a commercial fiber orientation analysis tool has shown no significant deviation. The resulting planar orientation distributions for two of the investigated fiber volume fractions are compared to the corresponding RVEs in Fig. 8. No CT data was available for the lowest volume fraction. The RVE of the volume fraction of 3.8 % (PPGF10) was therefore generated with the orientation distribution of the 8.2 % (PPGF20) material. The fiber meshes of the variants with the medium and highest fiber volume fraction are compared to the respective CT scans in Fig. 9.

4.2. Experimental determination of fiber length distribution

The fiber length distribution cannot be determined from the CT scans since this would require identification of continuity of fibers which is not currently possible for LFT materials. The fiber length distribution was therefore determined by the analysis of the fiber lattice of an incinerated specimen with 13.2 % volume fraction (PPGF30) by means of automatic image analysis. The specimen was taken from the same region of the plate as the tensile as well as the CT specimens. A characteristic sample of fibers taken from the incinerated specimen was analyzed by an automatic scanning procedure. Photographs were taken after the fibers have been dispersed in a dilute solvent which were then analyzed by image processing software. The analysis was carried out by *xyz* *high precision* under application of the company's fiber separation procedure and analysis software *FASEP*® [23,24]. To distort the measurement as little as possible a large specimen area of approx. 100 x 60 mm was chosen to extract the fiber lattice. The resulting length distribution (weighted by length) is depicted in Fig. 10. The mean fiber length (weighted by length) is 15.2 mm. 8868 fibers have been analyzed. The original length distribution as received from the analysis features 80 length classes which turned out to be too fine to realize both orientation distribution and length distribution in the FE model with a reasonable number of fibers. The original length distribution has therefore been coarsened to only 33 length classes with a length interval of 200 µm for fibers below 2 mm length and a length interval of 2 mm from 2 - 48 mm fiber length. No significant deviation in mean weighted fiber length could be observed comparing the original and coarsened distributions.

4.3. Experimental determination of the fiber volume fraction

The fiber volume fraction was calculated from values for mass flow rates of the production process under consideration of the mass density values for fiber and matrix as specified in the manufacturer's data sheet [25,26]. The values for the three produced material variants are 3.8 % (PPGF10), 8.2 % (PPGF20) and 13.2 % (PPGF30).

4.4. Elastic properties, experimental

To measure the elastic properties of the LFT material, tensile tests with a strain rate of 22 10^{-5}/s were carried out with a *Hegewald&Peschke Inspekt 100* testing machine on specimens cut from the 3 mm thick plates. The dog bone shaped specimens with a reduced section of 70 x 10 mm² and a gauge length of 50 mm were taken from the flow region of the plate under 0° and 90° relative to the material's flow direction. The stiffness was determined from the initial, linear elastic part of the stress-strain curve, where no effects of plasticity or damage could be observed. At least three specimens per orientation were tested to obtain the stiffness values in flow direction E_1 and in transverse direction E_2. The values are presented in Table 1.

4.5. Elastic properties, numerical

Three RVE variants were generated to model the LFT material with all investigated fiber volume fractions. The specifics of the analyzed structures are shown in Table 2. The edge length of the square fiber cross section was chosen so that the numerical fibers had approximately the same cross sectional area as the real ones with a mean value of 17 µm diameter. The RVE dimensions were chosen to their specified values in order to realize the statistical data as well as possible, but keeping the maximum element count below the limit of 10 million elements. Aim of the numerical studies was to include the complete fiber length spectrum in mean fiber orientation direction. This is why an RVE dimension of 50 mm was chosen in *1*-direction. To limit the element count and for computational performance the *2*-direction was cropped to a much smaller value (1.5 mm for the highest volume fraction and 2.75 mm for the others). This explains the mean weighted fiber length of the generated structures being significantly below the experimental value of 15.2 mm (Table 2).

The elastic properties of matrix and fibers were set to the values specified in the manufacturer's data sheet [25] respectively to values taken from literature [27,8,11]. The values are E_m = 1250 MPa, ν_m = 0.35, E_f = 72 000 MPa, ν_f = 0.22. The resulting effective elastic properties of the three composites are presented in Table 1 together with the experimental and analytical data.

4.6. Elastic properties, analytical

With respect to analytical validation, the orientation averaging scheme after Advani and Tucker [7] has been applied to the LFT material data in the same form as described by Garesci [9] for a similar material. The same values for the constituent properties (E_m, ν_m, E_f, ν_f) as well as the microstructural data (fiber orientation distribution, fiber length distribution, fiber volume fraction) have been used as for the numerical approach. In order to apply the orientation averaging scheme, it was necessary to convert the planar fiber orientation distributions into second and fourth order orientation tensors. For this purpose, the periodic function $y = a \exp [b \sin(cx+d)] + e$ with the parameters a, b, c, d, e has been fitted to the experimental orientation data and has then been used to derive the tensor formulation in analogy to the procedure described by Garesci [9]. No significant deviation between experimental / numerical data and the fit functions can be observed in Fig. 8, where also the resulting second order orientation tensors a_{ij} are specified. The stiffness values obtained by application of the orientation averaging scheme have been analyzed for discrete values of aspect ratio of 10, 50, 100, 500, 1000, 2000, 3000 and 4000 for each volume fraction of 3.8 % (PPGF10), 8.2 % (PPGF20) and 13.2 % (PPGF30). To obtain the final values as specified in Table 1, averaging with respect to fiber length has been performed by weighing the analytical stiffness value for a specific aspect ratio with the respective fiber length fraction of the fiber length distribution.

5. Discussion

For all three investigated fiber volume fractions, the micromechanical model is able to reproduce the experimental results within a maximum deviation below 10 % which can in general be rated as very promising. The deviation to the analytical approach is somewhat higher with the analytical values of E_1 systematically being lower than the numerical results and E_2 being higher. This is likely caused by a certain degree of underestimation of E_1 respectively overestimation of E_2 by the Halpin-Tsai equations for aspect ratios greater than 10 (E_1), which has been reported by Tucker *et al.* by systematic comparison of the results of analytical and numerical models for unidirectional fiber composites [1]. Three general sources of uncertainty could be identified for the modeling procedure and are discussed in the following (5.1.-5.3). In the end, an assessment regarding the model’s potential is given in 5.4.

5.1. Characteristic values of the microstructure

The characteristic values of the microstructure have been determined by random samples. The CT screening section of 3³ mm³ used to extract the fiber orientation distribution can be considered as relatively small compared to the analysis section of the tensile specimens of 50 x 10 x 3 mm³. A possible variation of the orientation distribution within the specimens is not considered in the current data. Other uncertainties remain concerning the correlation between fiber length and orientation distribution. Experimental determination of such correlation is currently not possible since the orientation distributions and length distributions are determined by different and independent measurements, which cannot be related. It was therefore necessary to assume that the longest fibers are preferably aligned in flow direction for the generation of the fiber structures. (Although this assumption seems reasonable it is not validated by independent measurement.) In the generation procedure this is expressed by the finite number of attempts to re-orient a fiber preserving its length (see Section 3.1. for details). This re-orientation only affects the correlation between length and orientation distribution but does not modify the orientation distribution itself.

The uncertainty with respect to the fiber volume fraction can be considered as low. Appropriate studies based on weighing incinerated specimens demonstrated that the calculated values are sufficiently accurate for materials like the one investigated here [18]. For example, analysis of a 400 x 400 mm² specimen plate produced by compression molding with a nominal volume fraction of 13.2 % (30 wt-%) revealed a minimum value of 12.4 % and a maximum value of 13.8 % [28]. For most regions of the plate, the agreement to the calculated value was much better.

5.2. RVE dimensions and boundary conditions

It is remarkable that the numerical values for stiffness in flow direction E_1 show a smaller relative error to the experimental data than the values for E_2. The applied method of homogenization induces that every fiber long enough to connect the analysis node sets (Fig. 5) contributes to the overall stiffness in an equivalent way as an endless fiber. In *1*-direction, the distance between the node sets (40 mm) is very close to the stiffness saturation length with the result that the applied method of volume averaging is accurate. In detail, fibers longer than 40 mm which are incorrectly considered as endless do not significantly affect the effective properties since the stiffness of a 40 mm fiber (aspect ratio 2350) represents approx. 99 % of the saturation value according to the Halpin-Tsai equations [6]. However, the distance between the node sets in *2*-direction is significantly smaller (approx. 2 mm for 3.8 and 8.2 % volume fraction (PPGF10/PPGF20), 1 mm for 13.2 % (PPGF30)) so that a substantial amount of fibers is overrated in their contribution to the overall stiffness. Evaluation of the Halpin-Tsai equations [6] reveals that a 1 mm fiber (aspect ratio 60) represents approx. 75 % and a 2 mm fiber (aspect ratio 120) approx. 85 % of the stiffness saturation value. It needs to be mentioned that for prediction of the elastic stiffness in both directions within engineering accuracy, a quadratic RVE base section of e.g. 5 x 5 mm^2 would be unproblematic with respect to the element count and still be suited to include the most relevant part of fiber length up to 93 % of the saturation value. However, the RVEs of this work have been generated with respect to application beyond linear elasticity where no such saturation length might exist. Hence the implementation of the asymmetric RVE dimensions is currently the only way to incorporate the complete fiber length spectrum in *1*-direction while it must be accepted that the *2*-direction gives somewhat less accurate results.

5.3. Mesh effects

Another reason for deviations between numerical and experimental results might be the effect of the relatively coarse mesh and in particular the representation of the matrix by linear tetrahedral elements which were chosen for computational performance. Such linear elements are known to be less accurate at stress and strain concentrations which arise e.g. at the end of a fiber. This is partially addressed by the meshing algorithm which decreases the element size in regions close to a fiber and increases the size towards regions of low fiber density, where no strain concentrations are present. An element study was performed on a smaller structure (1 x 1 x 0.2 mm^3). The original mesh used to analyze the large RVEs (1 linear hexahedral element with reduced integration C3D8R by fiber cross section, linear tetrahedral elements C3D4 for the matrix) was compared to a quadratic variant (2 quadratic tetrahedral elements C3D10 by fiber cross section, quadratic tetrahedral elements C3D10 for the matrix). The original mesh was found to be 6 % stiffer than the quadratic mesh. This is considered as a rather moderate deviation.

5.4. Potential of the modeling approach

It has been shown that the 3D model predicts the elastic properties of all three investigated materials with less than 10 % deviation from experimental data. In contrast to analytical approaches which are mostly based on a unidirectional reference composite, fiber waviness and entanglements as a result of the dense packing are inherent to the 3D approach. However, the simplifications of the analytical approach do not affect significantly the elastic properties, thus the results of the orientation averaging scheme [7,9] presented in Table 1 are in good agreement to experimental and numerical results. While analytical approaches require assumptions for the length averaging that are still controversially discussed, the FE model does not require such assumptions since the effects of fiber length are explicitly computed. For example, the number average length has been found to be most accurate comparing analytical to 3D models for short fiber composites [11], whereas implementation of the weighted length distribution yields better results for injection molded LFTs [8]. Nevertheless, the established analytical models are accurate enough to predict elastic properties and thus the tremendous effort of the 3D approach does not seem to be well justified. Applications beyond linear elasticity can thus be considered as the true potential of the 3D approach. Contrary to the analytical models, the 3D approach provides detailed information about the stress-strain state at the microscopic level. Thus, the effects of stress concentration, localization and progressive damage of matrix, fibers and the interface can be described in conjunction with fiber-fiber interactions resulting from the complex geometry and with the nonlinear deformation behavior of the matrix. Whereas the fiber length rather weakly affects the elastic properties, its influence on the damage behavior is of much greater interest. Hence the model can be helpful to identify the optimum microstructure for a given application and to understand the complex deformation and damage behavior of LFTs. Validation with respect to the elastic properties as carried out in this work was just the first necessary step to establish the model. Application to non-linear behavior beyond the capability of analytical approaches is our aim. Hence, new effective models for LFT, suitable for the structural simulation of parts or components can be developed and validated with the help of detailed microstructural models such as the one introduced here.

6. Conclusions

With the presented RVE generation procedure, a rather effective way was found to model the complex microstructure of LFT including the complete fiber length spectrum. In contrast to the established analytical models, the procedure considers effects of geometrical features like fiber waviness and can be extended to include the complex, non-linear behavior of a thermoplastic matrix and to account for interface and/or material damage effects. Validation against experimental data showed excellent agreement for all three investigated materials with different fiber volume fractions. Although simplifications as the rather coarse mesh and assumptions concerning the correlation between length distribution and orientation distribution had to be made in order to keep within the limits of computational performance, the approach can generally be considered as promising to model materials with a microstructure similar to the one investigated here.

7. Acknowledgements

Financial support of the *KITe hyLITE* innovation cluster is gratefully acknowledged. The authors would like to thank B. Hangs at Fraunhofer ICT for providing the material, R. Schlimper at Fraunhofer IWM for CT analysis and F. Garesci at University of Messina for implementation of the orientation averaging scheme.

8. References

[1] Tucker CL, Liang E. Stiffness predictions for unidirectional short-fiber composites: Review and evaluation. Comp. Sci. Tech. 59 (1999) 655-671

[2] Eshelby JD. The determination of the elastic field of an ellipsoidal inclusion and related problems. Proc. Roy. Soc. A 241 (1957) 376-396.

[3] Mori T, Tanaka K. Average stress in matrix and average elastic energy of materials with misfitting inclusions. Acta Metallurgica 21 (1973) 571-574.

[4] Tandon GP, Weng GJ. The effect of aspect ratio of inclusions on the elastic properties of unidirectionally aligned composites. Polym. Compos. 5 (1984) 327-333.

[5] Hill R. Elastic properties of reinforced solids: Some theoretical principles. J. Mech. Phys. Solids 11 (1963) 357-372.

[6] Halpin JC, Kardos JL. The Halpin-Tsai Equations: A Review. Polymer Engineering and Science 16-5 (1976) 344-352.

[7] Advani SG, Tucker CL. The use of tensors to describe and predict fiber orientation in short fiber composites. Journal of Rheology, 31 (1987) 751–784.

[8] Nguyen BN, Satish KB, Holbery JD, Smith MT, Kunc V, Frame BJ, Phelps JH, Tucker CL. Fiber length and Orientation in Long-Fiber Injection-Molded Thermoplastics – Part I Modeling of Microstructure and Elastic Properties. Journal of

Composite Materials 42 (2008) 1003-1029.

[9] Garesci F, Fliegener S. Young's modulus prediction of long fiber reinforced thermoplastics. Comp. Sci. Tech. 85 (2013) 142-147.

[10] Gusev A, Heggli M, Lusti HR et al. Orientation averaging for stiffness and thermal expansion of short fiber composites. Adv. Eng. Mat. 4 12 (2002) 931-933.

[11] Hine PJ, Lusti HR, Gusev AA. Numerical simulation of the effects of volume fraction, aspect ratio and fibre length distribution on the elastic and thermoelastic properties of short fibre composites. Comp. Sci. Tech. 62 (2002) 1445-1453.

[12] Pan Y, Iorga L, Pelegri AA. Numerical generation of a random chopped fiber composite RVE and its elastic properties. Comp. Sci. Tech. 68 (2008) 2792-2798.

[13] Pan, Y. Stiffness and progressive damage analysis on random chopped fiber composite using FEM. Dissertation. The State University of New Jersey, 2010.

[14] Harper LT, Qian C, Turner TA, Li S, Warrior NA. Representative volume elements for discontinous carbon fibre composites - Part 1: Boundary conditions. Comp. Sci. Tech 72 (2012) 225-234.

[15] Soltani P, Johari MS, Zarrebini M. Effect of 3D fiber orientation on permeability of realistic fibrous porous networks. Powder Technology, 254 (2014) 44-56.

[16] Faessel M, Delisee C, Bos F, Castera P. 3D Modelling of random cellulosic fibrous networks based on X-ray tomography and image analysis. Comp. Sci. and Tech 65 (2005) 1931-1940.

[17] Henning F, Ernst H, Brüssel R, Geiger O, Krause W. LFTs for automotive applications. Reinforced Plastics 49 (2005) 24-33.

[18] Tröster S. Materialentwicklung und –charakterisierung für thermoplastische Faserverbundwerkstoffe im Direktverfahren. Dissertation, Fraunhofer Institut für Chemische Technologie, 2003. ISBN 3-8167-6643-9. (in German)

[19] Evans KE, Gibson AG. Prediction of the maximum packing fraction achievable in

randomly oriented short-fibre composites. Comp. Sci. Tech. 25 (1986) 149-162.

[20] S. Toll. Packing mechanics of fiber reinforcements. Polymer Engineering and Science, 38(8) 1337-1350, 1998.

[21] Tinevez J. Directionality plugin for ImageJ. http://fiji.sc/wiki/index.php/Directionality. 2013-12-09.

[22] Graupner N, Beckmann F, Wilde F, Muessig J. Using synchrotron radiation-based micro-computer tomography for the measurement of fibre orientations in cellulose fibre-reinforced polyactide composites. J Mater Sci 49 (2014): 450-460.

[23] xyz high precision. FASEP® fiber separation and analysis of length distribution. http://www.fasep.de, 2014-01-13.

[24] Hartwich MR, Hoehn N, Mayr H, Sandau K, Stengler R. FASEP ultra-automated analysis of fibre length distribution in glass-fibre-reinforced products. In Society of Photo-Optical Instrumentation Engineers (SPIE) Conference, Vol. 7389, p. 66, 2009.

[25] DOW® Chemical Company. C711-70RNA Polypropylene Resin. Product Information, 2003.

[26] PPG Fiber Glass. TufRov® 4575. Data Sheet, 2013.

[27] Gommers B, Verpoest I, Van Houtte, P. Modelling the elastic properties of knitted-fabric-reinforced composites. Comp. Sci. Tech. 56 (1996) 685-694.

[28] Radtke A. Steifigkeitsberechnung von diskontinuierlich faserverstärkten Thermoplasten auf der Basis von Faserorientierungs- und Faserlängenverteilungen. Dissertation, Fraunhofer Institut für Chemische Technologie, 2008. ISBN 978-3-8167-7852-3. (in German)

9. Figures

Figure 1: Structure of the fiber generator tool to create a stack of planar, straight fibers according to the given fiber orientation distribution and fiber length distribution.

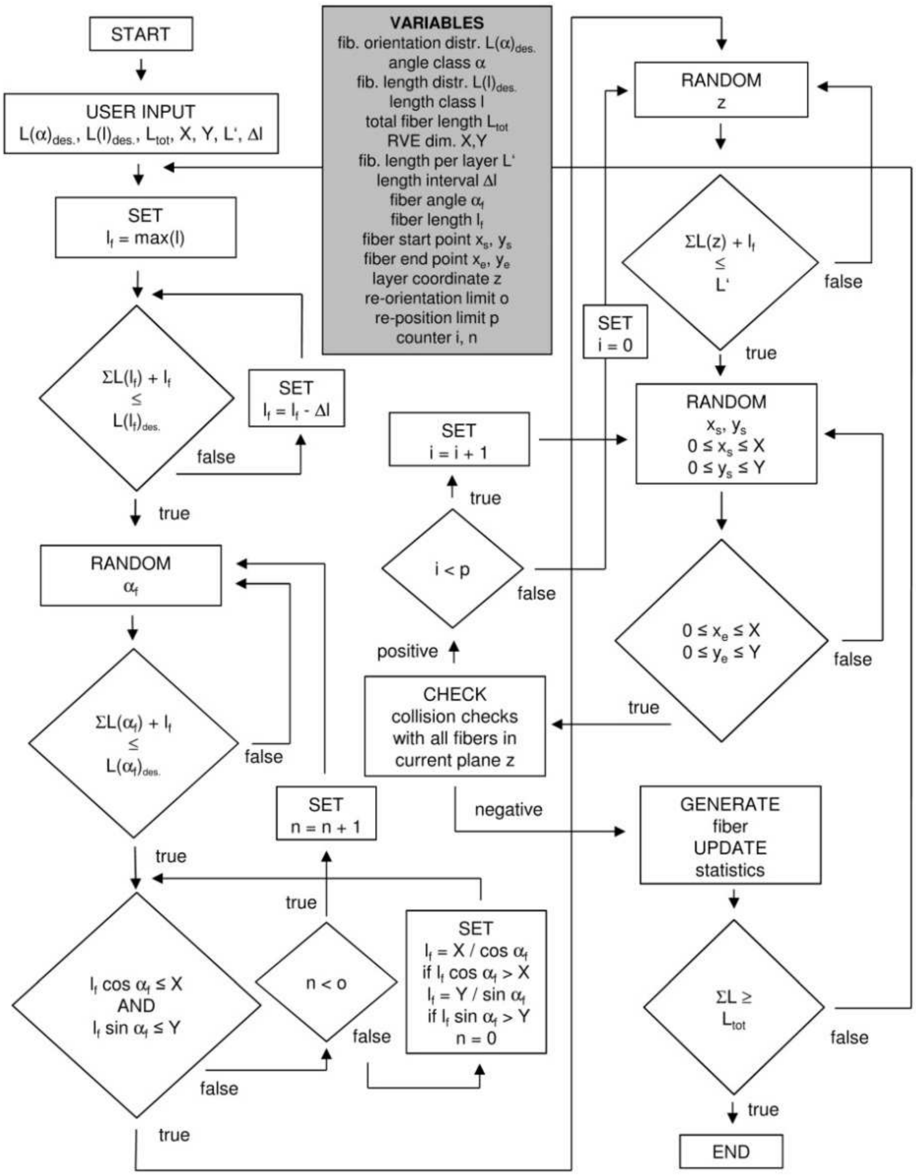

Figure 2: Fiber compression scenario showing the maximum displacement of the pressing plates u_{max} as well as the flow *(1)*, transverse *(2)* and the pressing direction *(3)*.

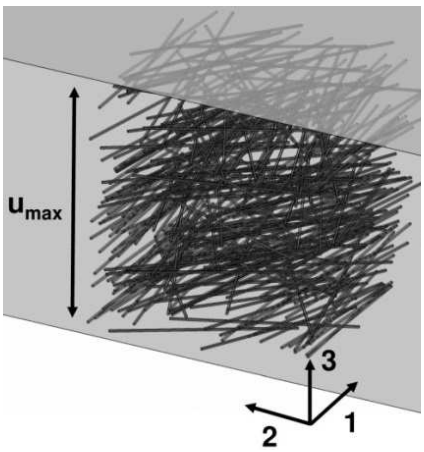

Figure 3: Mesh details of the RVE variants with different fiber volume fractions. Some of the matrix elements have been removed for illustration purposes.

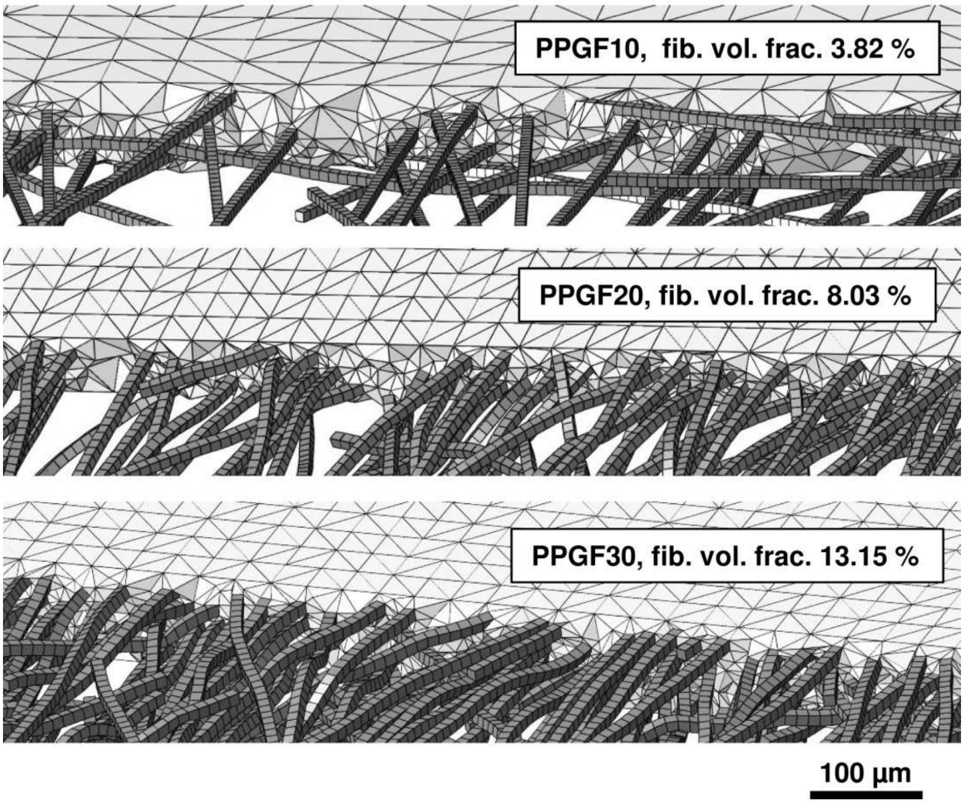

Figure 4: Details of the analyzed fiber structures with varying fiber volume fractions. One quarter of the RVE size is shown for each variant. All matrix elements have been removed.

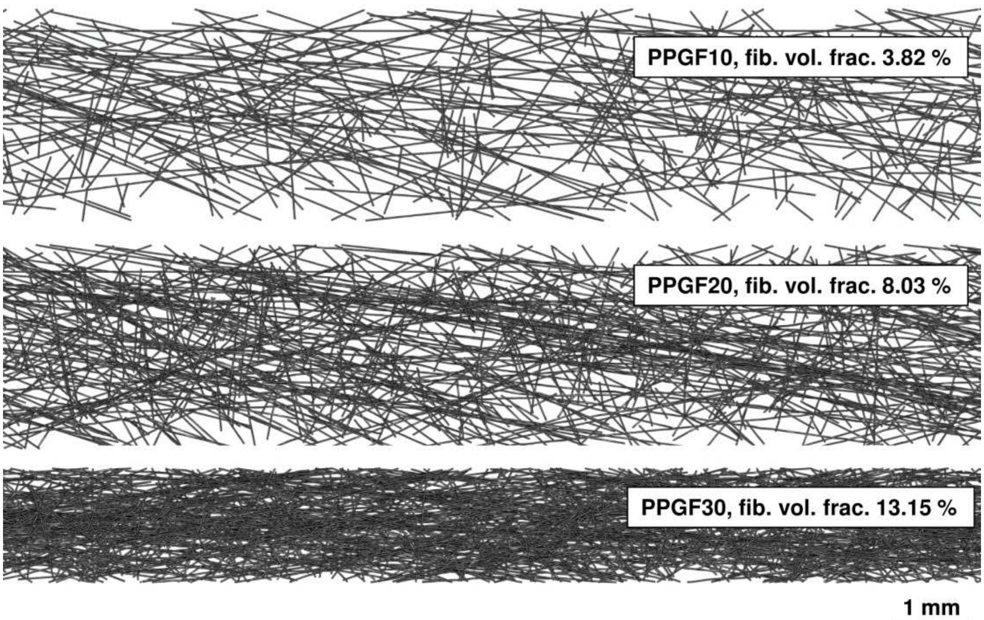

Figure 5: Applied BCs to determine the elastic properties of the RVEs. The displacement values for all nodes of each RVE border $u_1, \ldots, u_n$ are set to zero for one side and to a non-zero value for the opposite side. The node sets outside the stress concentrations are used to determine the averaged effective properties.

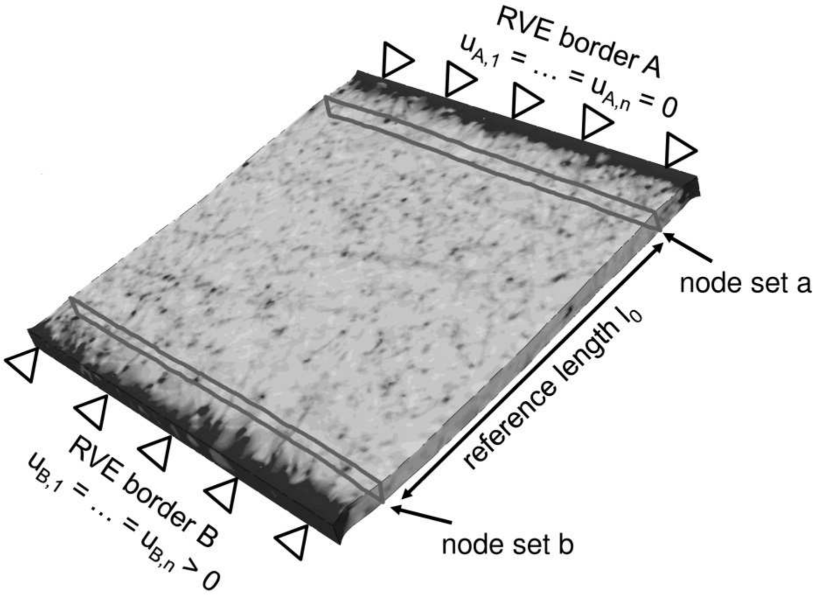

Figure 6: Analysis procedure to extract the fiber orientation distribution from CT scans: Raw CT voxel data (left, the arrow shows the flow direction), decomposition into a stack of 360 2D images (middle, exemplary image shown) and binarization and orientation analysis of each 2D image with the *Directionality* plugin of *ImageJ* (right). The data of the PPGF30 material (13.2 vol-%) is shown.

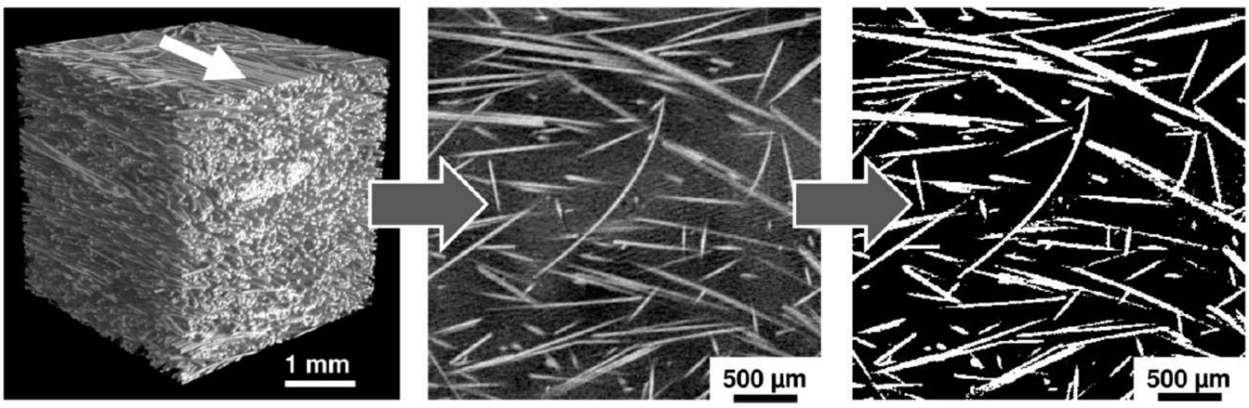

Figure 7: Plot of fiber orientation distribution over the image stack of 360 2D images of the PPGF30 material (13.2 vol-%). The black line represents the integral planar orientation distribution used for numerical and analytical models, as obtained by averaging over the 360 histograms of the stack.

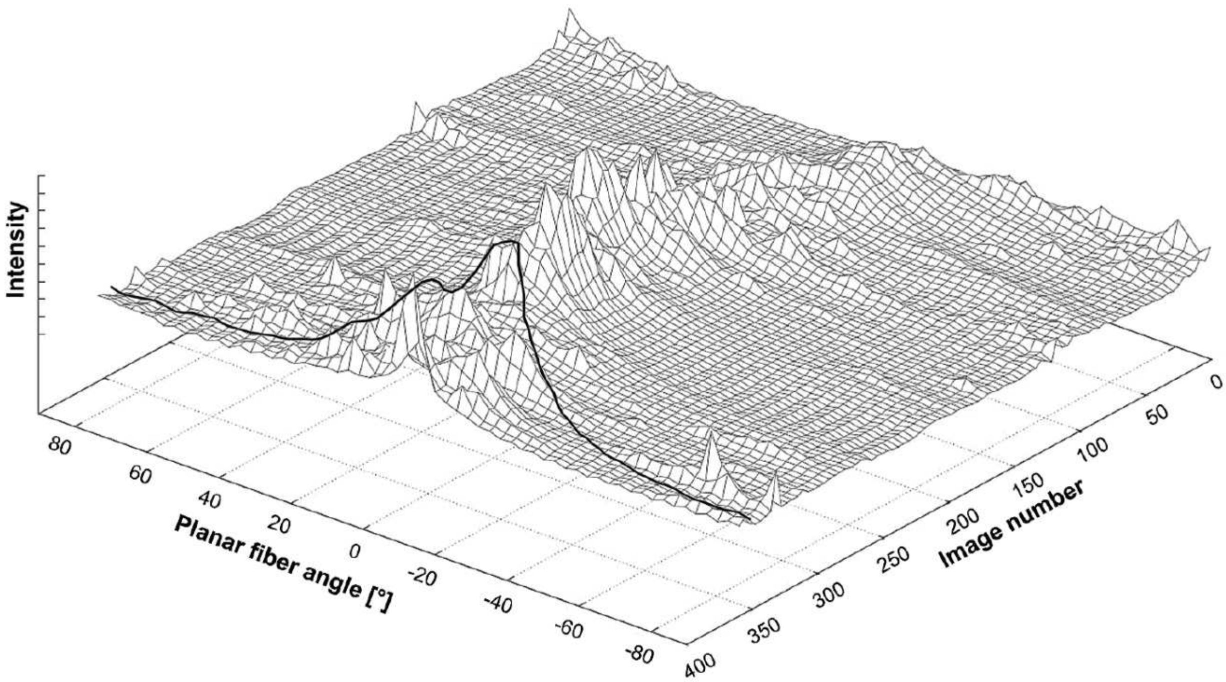

Figure 8: RVE orientation distributions compared to corresponding CT measurements and analytical fit functions used to calculate the fiber orientation tensors.

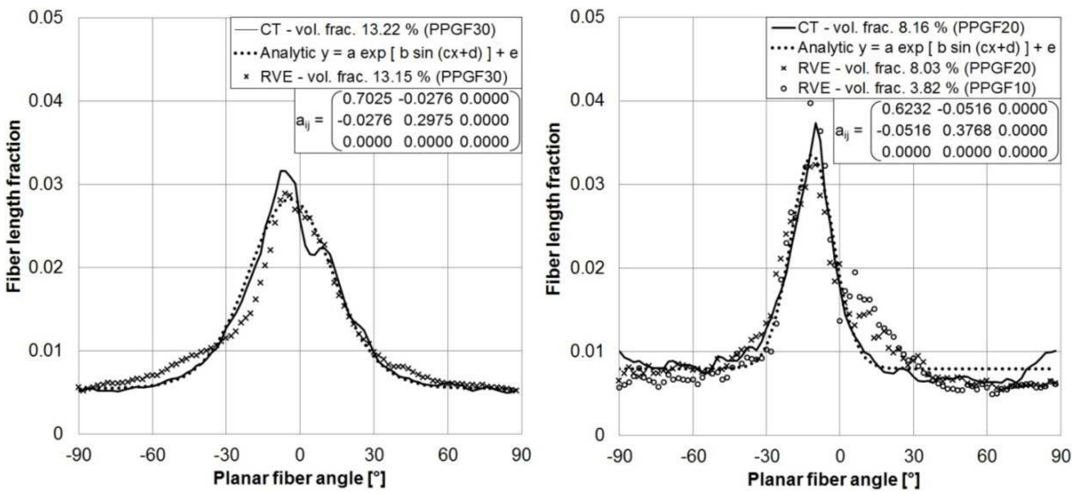

Figure 9: Comparison of CT scans and fiber meshes for two values of volume fraction.

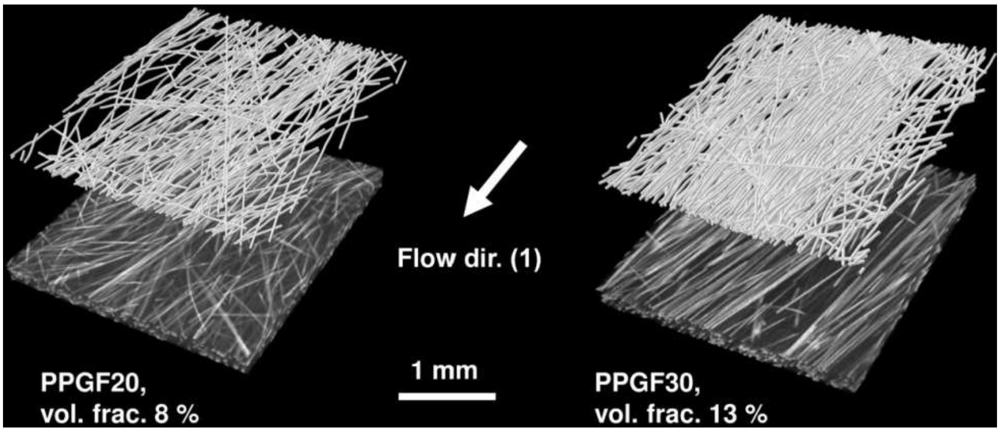

Figure 10: Fiber length distribution (weighted by length) as determined by analysis of an incinerated specimen with a fiber volume fraction of 13.2 % (PPGF30) [23,24].

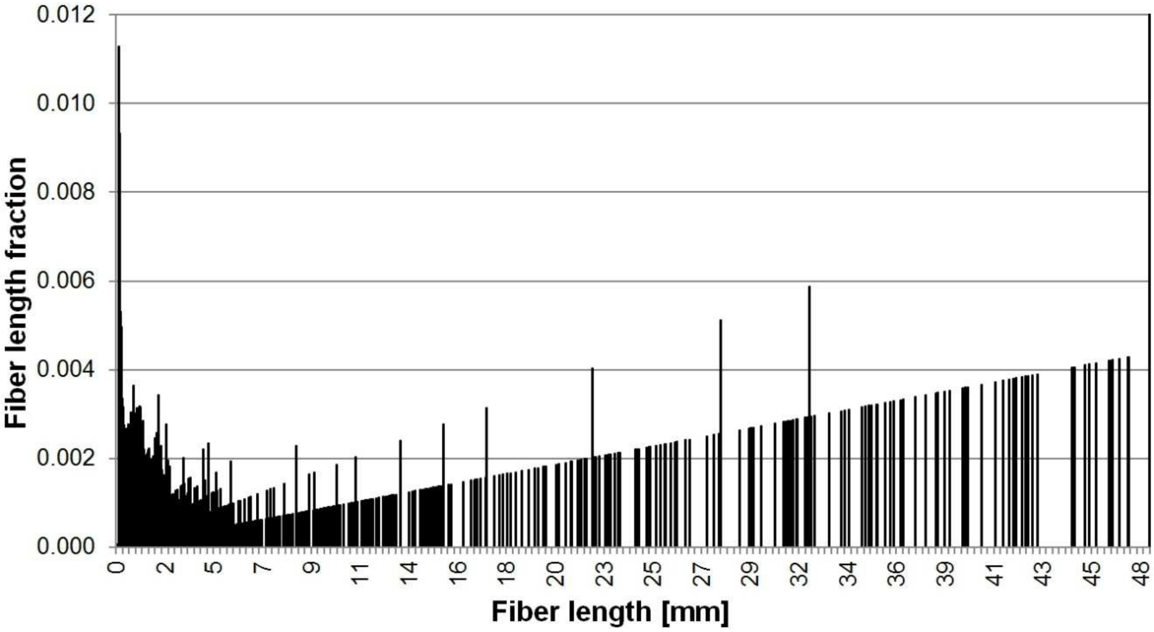

10. Tables

Table 1: Comparison of experimentally, numerically and analytically [7,9] determined elastic moduli.

Material	Vol. frac. exp. [%]	Vol. frac. num. / an. [%]	E_1 exp. [MPa]	E_1 num. [MPa]	E_1 an. [MPa]	E_2 exp. [MPa]	E_2 num. [MPa]	E_2 an. [MPa]
PPGF10	3.80	3.82	3052	2968	2568	2054	1999	2000
PPGF20	8.16	8.03	4435	4431	4025	2432	2568	2841
PPGF30	13.22	13.15	6649	6841	6508	3074	3148	3323

Table 2: Properties of the analyzed RVE variants.

Material	Vol. frac. [%]	RVE dimensions [mm³]	Element count	Fiber count	Total fiber length [mm]	Mean weighted f. length [mm]
PPGF10	3.82	50 x 2.75 x 0.125	$7.39\ 10^6$	1633	3056	10.1
PPGF20	8.03	50 x 2.75 x 0.099	$8.73\ 10^6$	2605	5048	9.4
PPGF30	13.15	50 x 1.5 x 0.134	$9.66\ 10^6$	3256	6067	8.1